Supplementary Information

Biallelic *FRA10AC1* variants cause a neurodevelopmental disorder with growth retardation

Table of content page

Case reports

Patient 1

The girl is the fourth child of healthy consanguineous parents of Arabic descent. Her three sisters are healthy. One uncle had a heart defect; he died at the age of 5 years. A more distant family member had transposition of great arteries. The remaining family history was unremarkable. Intrauterine growth restriction and a complex heart defect were identified during pregnancy. Extensive prenatal genetic testing including karyotyping, array-CGH and sequencing of genes associated with heart defects revealed normal results. The girl was born at term via vaginal delivery with weight of 3018 g (-1.3 z), length of 48 cm (-1.9 z) and occipitofrontal head circumference (OFC) of 33 cm (-1.7 z). APGAR was 5/8/9. She was admitted to the NICU for further monitoring and diagnostic procedures. The diagnosis of complex heart defect was confirmed: she had pulmonary artery atresia, ventricle septum defect, persistent ductus botalli, and persistent foramen ovale. In addition, agenesis of the corpus callosum and large ventricles were detected in brain ultrasound, caudally located left kidney and echogenic signal of both kidneys in renal ultrasound, and punctuate echogenic signals in liver in abdominal ultrasound. Facial dysmorphism comprised nevus flammeus on the forehead, nose and philtrum, bitemporal narrowing, broad and medial flaring of eyebrows, upslanted and narrow palpebral fissures, hypertelorism, large mouth, retrognathia, full cheeks, and low-set posteriorly rotated ears (**Fig. 1B**). She had short neck and short sternum, ulnar deviation of the left hand, proximal placement of thumbs and bilateral clinodactyly of fifth finger. The clinical diagnosis of Bohring-Opitz syndrome was not confirmed by *ASXL1* sequencing. The course of disease was characterized by feeding difficulties requiring feeding tube and placement of G-tube at the age of 2 years and 2 months. She had various non-curative procedures and surgeries for the heart defect. At the age of two months, epilepsy started which was well controlled on medication. She showed slow development and sometimes regression. At the age of 3 years and 1 month, she was able to grasp and roll over. She was hypotonic and showed decreased spontaneous movements. She made some sounds but did not speak. Her measurements were 9.4 kg (-3.4 z) for weight, 85 cm (-2.8 z) for length and 45 cm (-4.1 z) for OFC. She showed contracture of the left elbow and patchy hypopigmentation on upper limbs.

Patient 2

This individual is a 9-year-old female of first cousin parents. She has a healthy male sibling. There was maternal history of unexplained single abortion at 4 weeks gestation. No positive family history of similar condition or other genetic diseases. The pregnancy history showed oligohydramnios and mild intrauterine growth retardation and the child was delivered by Caesarian section. The perinatal history was inconspicuous and Apgar score was 5/7/10 at 1/5/10 minutes. Birth weight was 2250 g (-2.7 z), length 47 cm (-2.0 z) and OFC was 32 cm (-2.5 z). Neonatal history showed feeding difficulties and

floppiness. Delayed milestones of development were recorded, the child could sit at 2 years, stand supported at 2 years and 6 months, and was able to walk at 3 years. No speech acquisition was present, she only vocalized and produced sounds. Sphincter controlled was not attained and she had no abilities to have any independent tasks except sometimes being able to drink by herself by holding her bottle. Irritability and sleepless were noted at age 4 years and treated by risperidone. On evaluation, patient 2 had autistic features, no words and no response to commands except in rare occasions. Her anthropometric measurements were weight of 15 kg (-5.3 z), height of 109 cm (-4.3 z) and OFC of 47 cm (-4.8 z). She showed long face, multiple brownish nevi scattered on nose and cheeks, high forehead, broad and medial flaring of eyebrows, narrow palpebral fissures, prominent nose, and low set ears (**Fig. 1B**). Clinodactyly was noted bilaterally in hands. Neurological examination revealed hypotonia with present reflexes. Other investigations revealed normal karyotyping, metabolic screening, organic acid in urine, abdominal ultrasound and echocardiography. CARS was estimated as 39 (mild-moderate autism) and IQ was 35 (profound intellectual disability). Brain MRI showed near total agenesis of corpus callosum, colpocephaly and a right retroorbital cyst (**Fig. 1B**).

Patient 3-1

This individual is a 15-year-old boy, the first child of healthy, consanguineous Egyptian parents with no significant family history of intellectual disability. This pregnancy was followed by a pregnancy with monozygotic twin males who died on postnatal day 2 and 3 because of respiratory distress. Patient 3-1 was born at full term with a birth weight of 2500 g (-2.6 z). Birth length and head circumference were not recorded. He sat without support at the age of 8 months and walked at the age of 15 months. At age 15 years, his weight, height and OFC were 32 kg (-3.9 z), 134 cm (-4.8 z) and 50.3 cm (-3.8 z), respectively. He had mild hypotonia on neurological examination but otherwise an unremarkable physical examination. Dysmorphic features included long face, synophris, hypertelorism, narrow palpebral fissures, high arched palate, thick lips, pointed chin (**Fig. 1B**). Additionally, clinodactyly of the fourth and fifth toes was noted. Parents noted delay in communication and language. He had no meaningful words until the age of 36 months and showed better receptive than expressive language abilities. He had mild intellectual disability with IQ score of 68 using Stanford-Bienet test. No history of behavioral problems or sleep disturbance was noted and seizures have never occurred at any stage of his life. The parents were concerned about the stagnation of growth. A growth hormone deficiency was documented via the Clonidine growth hormone stimulation test. The boy had normal hearing, vision, and cranial nerve function. Echocardiography, abdominal ultrasound and EEG showed normal results. Brain magnetic resonance imaging (MRI) showed normal brain architecture but thin stretched corpus callosum (**Fig. 1B**). Karyotyping and metabolic testing were normal.

Patient 3-2

Patient 3-2 is the younger brother of patient 3-1. He was born at term via uncomplicated vaginal delivery after an uneventful prenatal history. His birth weight was 1800 g (-4.2 z). After birth, he suffered from respiratory distress and was admitted to NICU for 11 days. During infancy, he was delayed in achieving early motor and language milestones. He began to walk at age 18 months. At age 10 years, his weight, height and OFC were 20.5 kg (-3.6 z), 113.5 cm (-4.2 z) and 49.4 cm (-3.1 z), respectively. Mild hypotonia on neurological examination was noted. He was able to speak single words at the age of $3^{4}/_{12}$ years. IQ score was 77 using Stanford-Bienet test. He had similar facial features as his older brother (**Fig. 1B**). He showed growth hormone deficiency. Brain MRI at this time revealed thin stretched corpus callosum.

Patient 3-3

This individual is the youngest brother of patients 3-1 and 3-2. He was born at term after an uncomplicated pregnancy and delivery. His birth weight was 2250 g (-3.1 z). Birth length and head circumference were not recorded and he had no complications during the neonatal period. The patient sat at age 7 months and walked unsupported at age 14 months. He had delayed speech. He was able to speak single words at the age of 2½ years. At 7 years of age, his weight was 19 kg (-1.8 z), height 109 cm (-2.9 z), and OFC 50 cm (-2.0 z). On physical examination, his dysmorphic features resemble those of his siblings (**Fig. 1B**). IQ score was 77 using Stanford-Bienet test. Brain MRI findings were similar to those of his siblings.

Supplementary figures

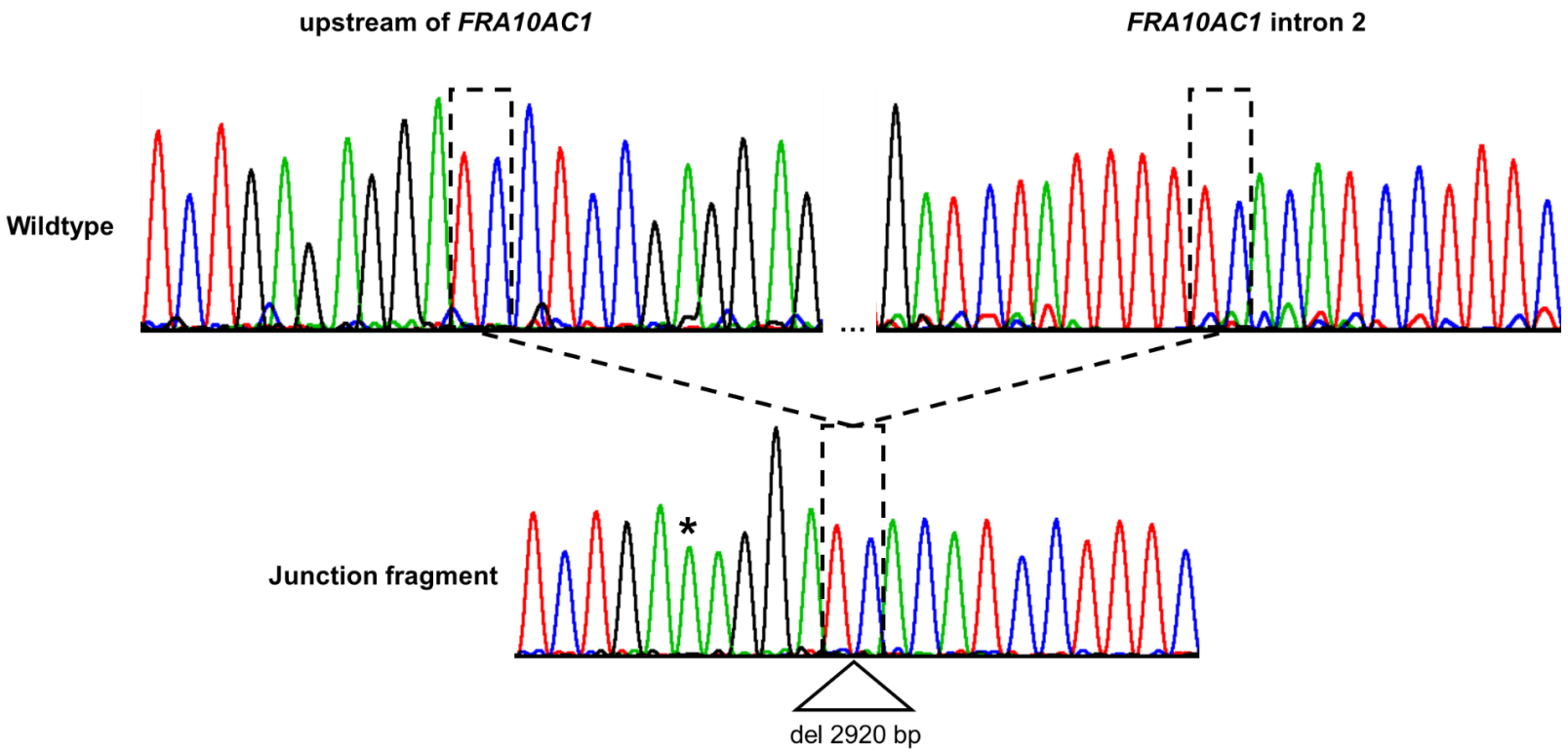

Supplementary Figure 1. Partial sequence electropherograms showing the breakpoint sequence of the 2.9-kb *FRA10AC1* deletion in leukocyte-derived DNA of patient 1

To validate the partial homozygous deletion in leukocyte-derived DNA of patient 1, the PCR-generated junction fragment was sequenced (lower panel). This confirmed a homozygous 2920-bp deletion on chromosome 10 encompassing exons 1 and 2 of the *FRA10AC1* gene. For control purposes, leukocyte-derived DNA of a healthy individual was used, and partial sequence electropherograms of the PCR fragment generated from the wild-type allele are shown (top panel). Deletion breakpoints with 2 bp overlap are indicated by dashed boxes (deletion coordinates: chr10:95,459,757-95,462,676 [hg19]). The asterisk marks a homozygous single nucleotide variant in the DNA of patient 1 (10:95,462,681C>T [hg19]).

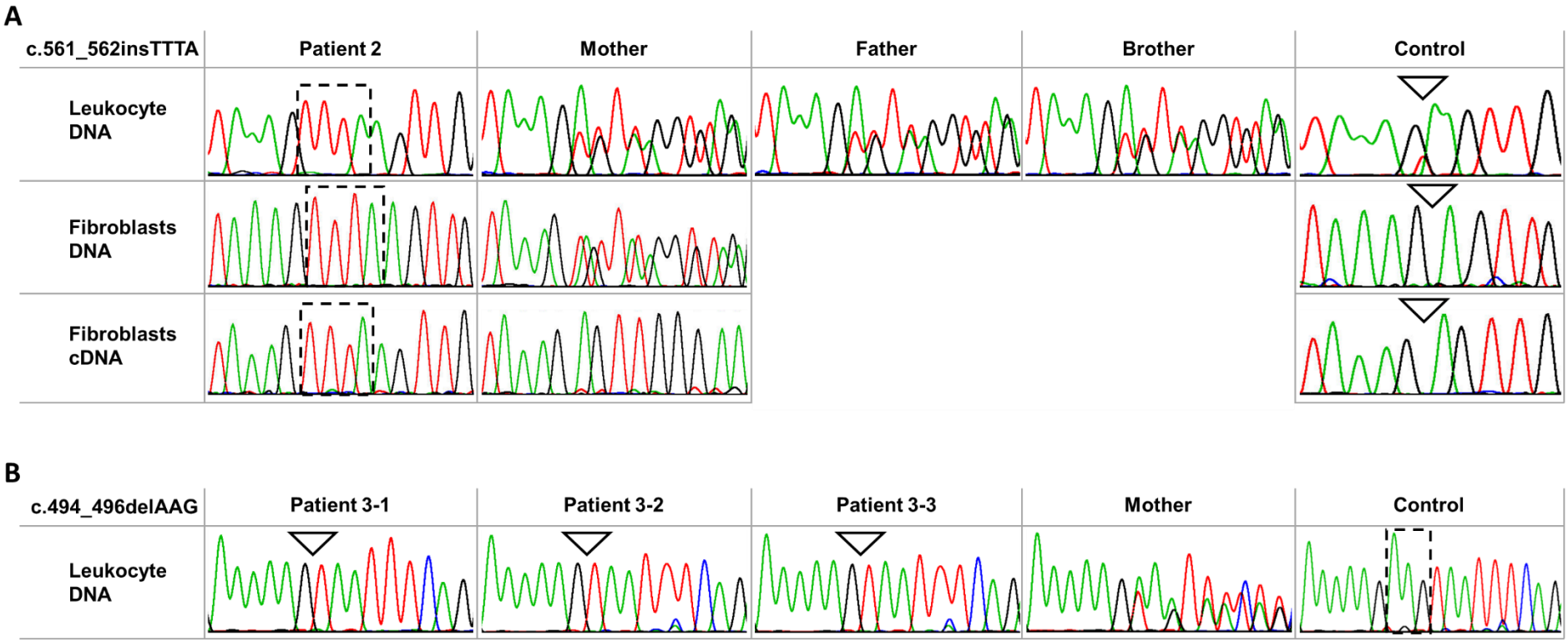

Supplementary Figure 2. *FRA10AC1* variant validation in DNA and/or cDNA of families 2 and 3

(**A**) Partial sequence electropherograms showing the presence of the *FRA10AC1* c.561_562insTTTA variant in leukocyte- and fibroblast-derived DNA and cDNA of patient 2 and her mother, and leukocyte-derived DNA of father and brother. Patient 2 is homozygous for the variant and healthy parents and brother are heterozygous carriers. Fibroblast-derived cDNA analysis shows the presence of mutated *FRA10AC1* mRNAs with the c.561_562insTTTA variant in patient 2 and predominant abundance of wildtype *FRA10AC1* transcripts in the mother, suggesting nonsense-mediated mRNA decay of transcripts harboring the insertion. For control purposes, fibroblast and leukocyte-derived DNA and/or cDNA of a healthy individual (control) was used, and respective sequence traces are shown.

(**B**) Partial sequence electropherograms showing the presence of the *FRA10AC1* c.494_496delAAG variant in leukocyte-derived DNA of patients 3-1, 3-2, 3-3, and their mother. All patients are homozygous for the variant, and the healthy mother is a heterozygous carrier. DNA of the healthy father was not available. For control purposes, leukocyte-derived DNA of a healthy individual (control) was used, and respective sequence trace is shown.

Triangles indicate the position of the insertion (A) or deletion (B), and the dashed boxes outline the 4-bp insertion (A) or the 3-bp deletion (B) in the DNA sequence.

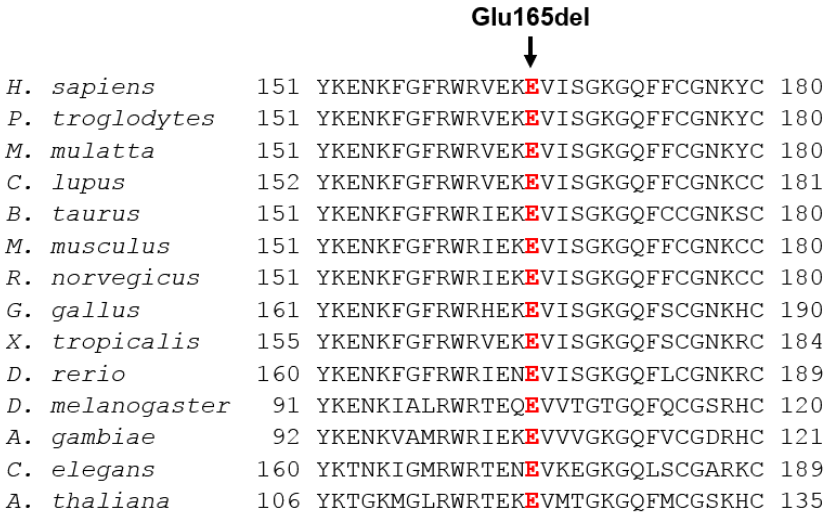

Supplementary Figure 3. Partial amino acid sequence alignment of FRA10AC1

Partial amino acid sequence alignment of human FRA10AC1 with orthologs shows evolutionary conservation of the deleted residue (highlighted in red) between species. For the alignment the following protein sequences were used: *Homo sapiens* (NP_660289.2); *Pan troglodytes* (XP_507931.2); *Macaca mulatta* (NP_001253649.1); *Canis lupus* (XP_534970.4); *Bos taurus* (NP_001069860.1); *Mus musculus* (NP_001074544.1); *Rattus norvegicus* (NP_001014268.1); *Gallus gallus* (XP_421674.1); *Xenopus tropicalis* (NP_001072824.1); *Danio rerio* (NP_001006006.1); *Drosophila melanogaster* (NP_723837.2); *Anopheles gambiae* (XP_311443.3); *Caenorhabditis elegans* (NP_001129806.1) and *Arabidopsis thaliana* (NP_193239.5). Sequence alignment was generated using CLUSTAL Omega (1.2.4) multiple sequence alignment.

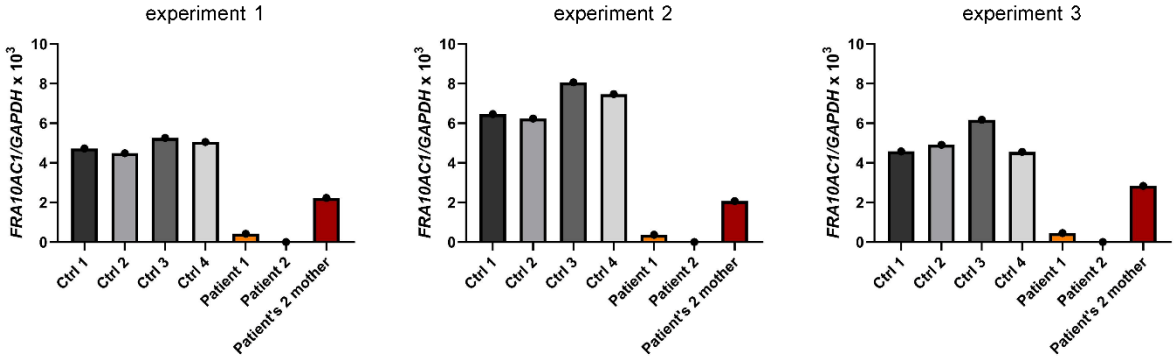

Supplementary Figure 4. Data set of three independent TaqMan gene expression assays shown in Figure 2C

Quantification of the relative *FRA10AC1* transcript levels in fibroblasts of patients 1 and 2, the mother of patient 2, and four controls by TaqMan gene expression assay. *GAPDH* mRNA was used as an internal control. Relative quantification was performed according to the ΔC_T method and results were expressed in the linear form using the formula $2^{-\Delta\Delta CT}$ and multiplied by a factor of 1000. Data sets from three independent experiments are shown.

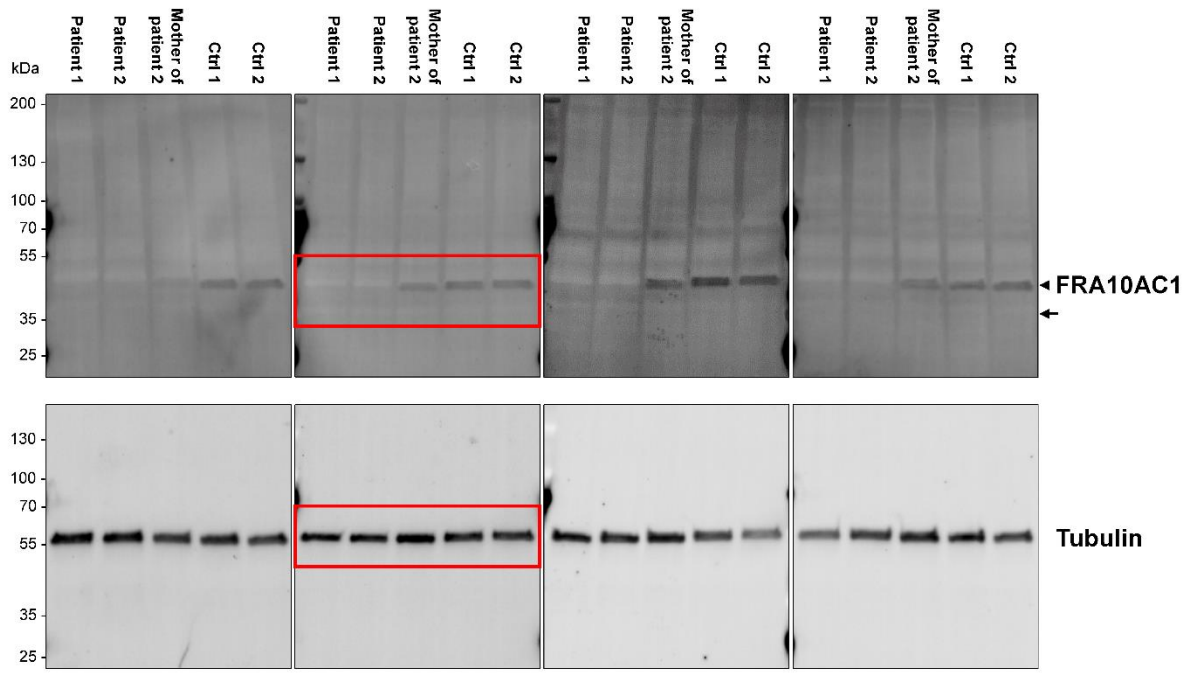

Supplementary Figure 5. Full-length immunoblots used for quantification of FRA10AC1 amount shown in Figure 2D

Full-length immunoblots of lysates obtained from fibroblasts of patients 1 and 2, mother of patient 2, and two healthy individuals from four independent experiments are shown. The amount of FRA10AC1 was detected by an anti-FRA10AC1 antibody. An anti-Tubulin antibody was used to demonstrate equal loading. The predicted molecular mass of FRA10AC1 is ~38 kDa (indicated by an arrow); endogenous FRA10AC1 had a molecular mass of ~45 kDa (indicated by an arrowhead). Red boxes indicate the cropped area.

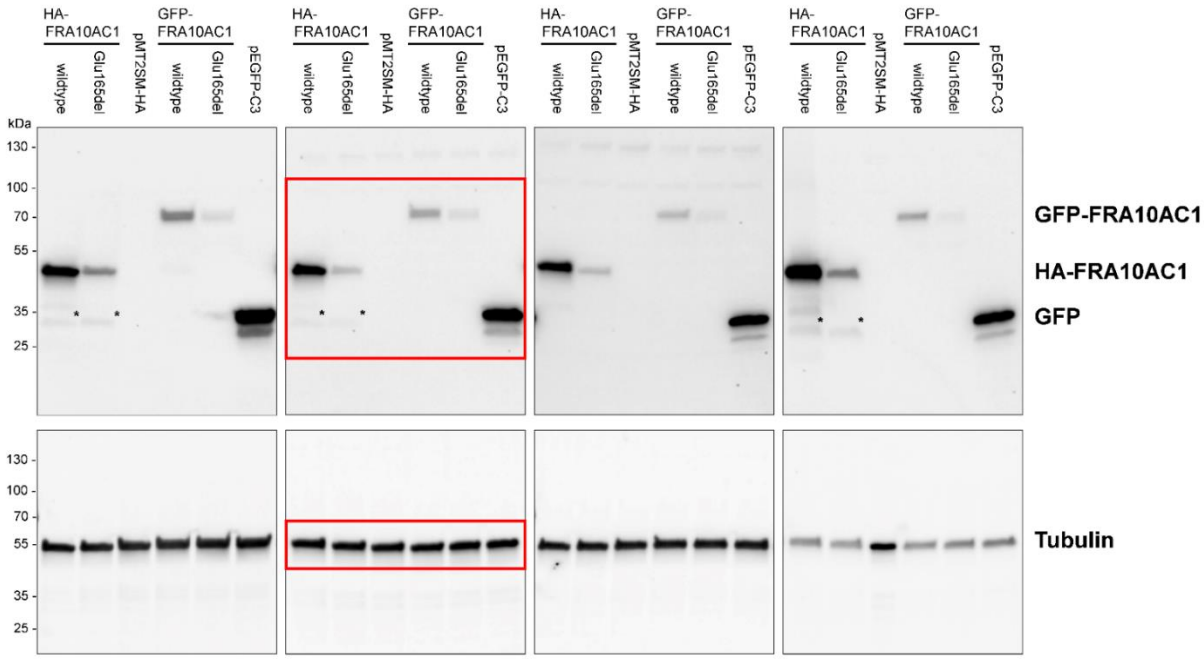

Supplementary Figure 6. Full-length immunoblots used for quantification of FRA10AC1 levels shown in Figure 3A

Full-length immunoblots of lysates obtained from HEK293T cells transfected with the indicated plasmids from four independent experiments are shown. FRA10AC1 protein was detected by using an anti-GFP or anti-HA antibody. An anti-Tubulin antibody was used to demonstrate equal loading. A non-specific band at ~30 kDa was observed with the anti-HA antibody (marked by asterisks). Red boxes indicate the cropped area.

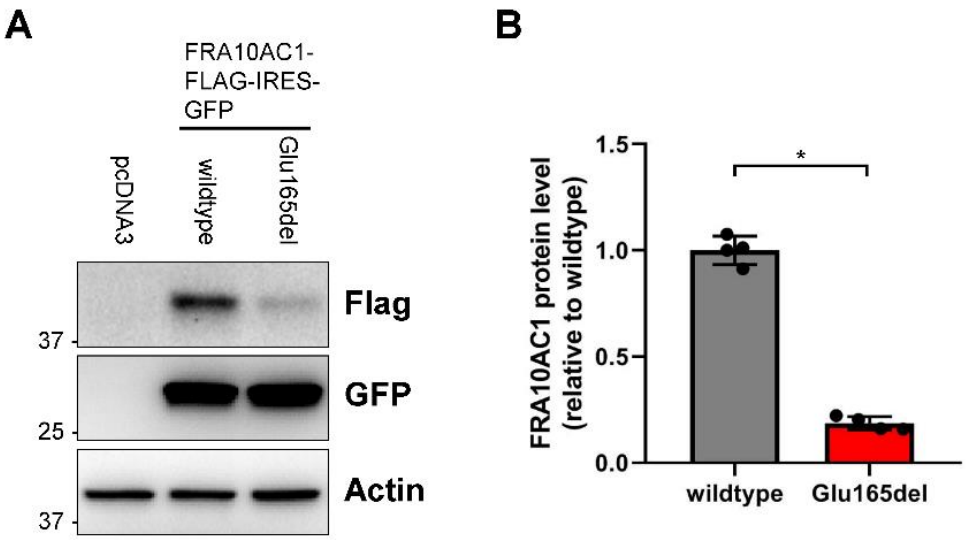

Supplementary Figure 7. Immunoblotting and quantification of C-terminally FLAG-tagged wild-type and Glu165del mutant FRA10AC1

(**A**) Immunoblot of lysates obtained from HEK293T cells transfected with pcDNA3.1(+) plasmids with FRA10AC1-FLAG-IRES-GFP. The amount of FRA10AC1 protein was monitored by immunoblotting using anti-FLAG and anti-GFP antibodies. An anti-Actin antibody was used for equal loading.

(**B**) Band intensities were quantified and normalized to wild-type protein amount. The mean ± SD of four technical replicates from two independent experiments is given. Mann-Whitney test was used for statistical analysis: * $P \leq 0.05$.

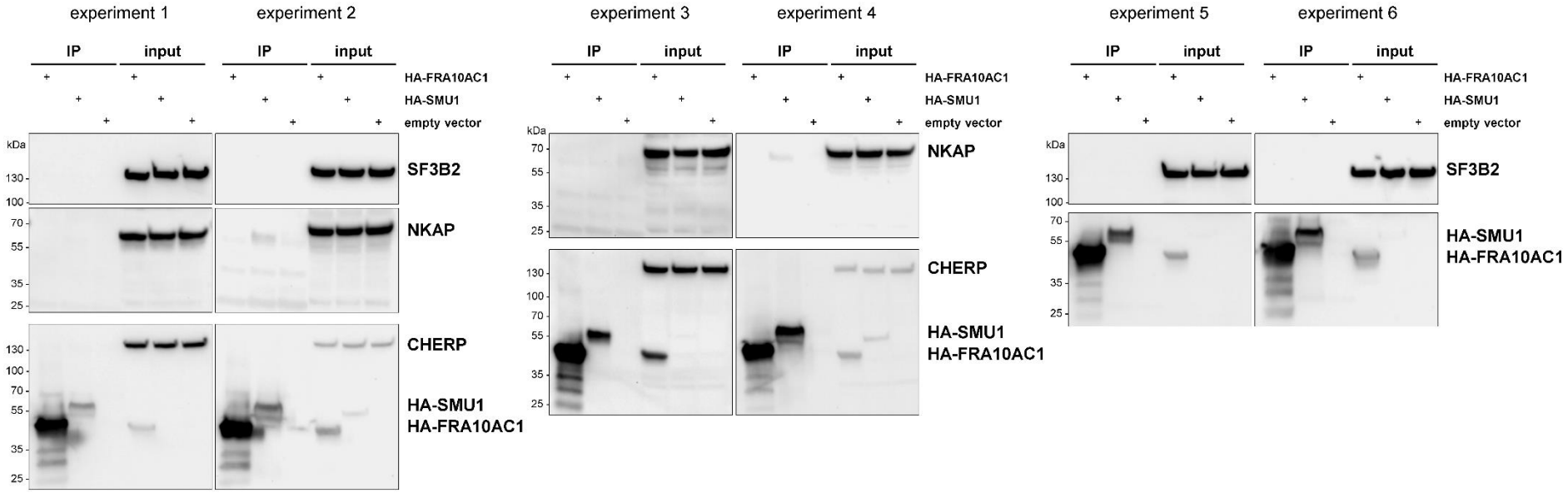

Supplementary Figure 8. Full-length immunoblots of co-immunoprecipitation of endogenous SF3B2, NKAP and CHERP with HA-FRA10AC1 or HA-SMU1

Full-length immunoblots of co-immunoprecipitation experiments performed with HEK293T cells transfected with the indicated plasmids from four independent experiments are shown. An empty vector (pMT2SM-HA) was used as a negative control. Co-precipitated endogenous splicing factors were detected by immunoblotting using anti-SF3B2, anti-NKAP, and anti-CHERP antibodies. HA-tagged proteins were monitored by HRP-coupled anti-HA antibody.

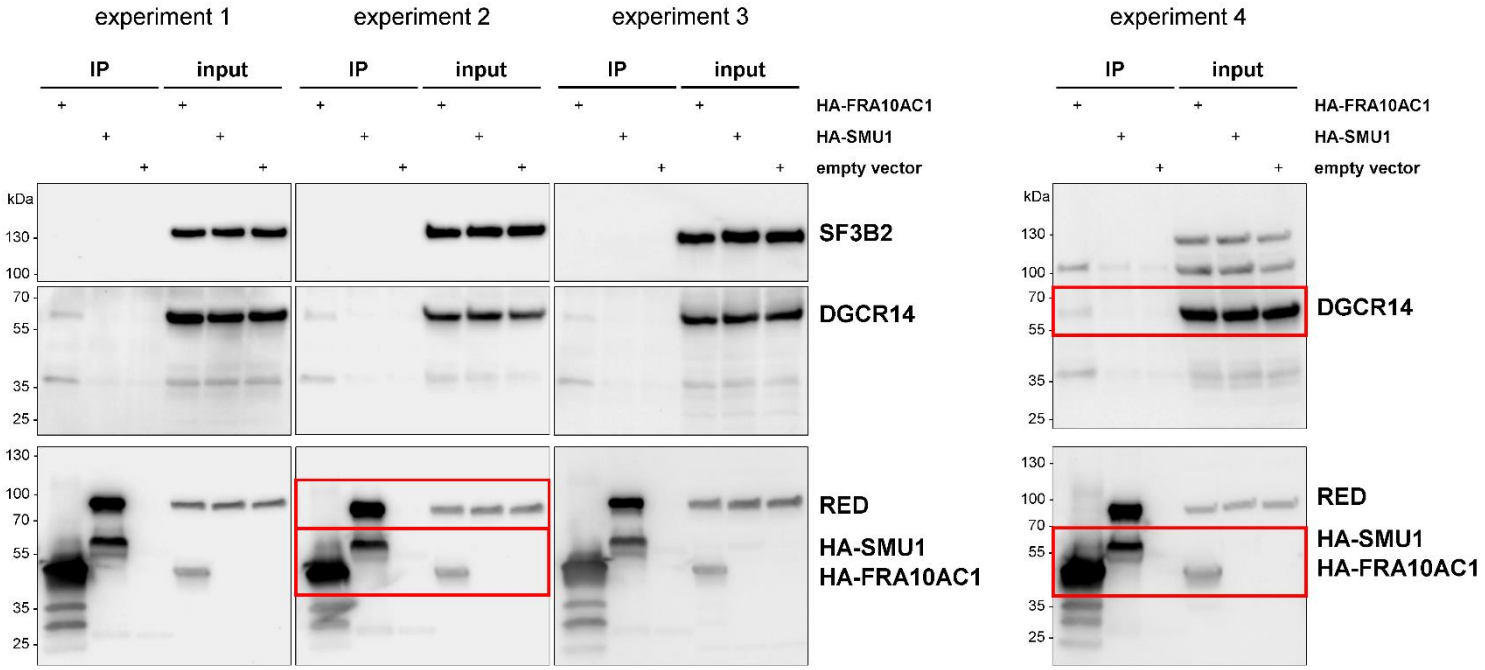

Supplementary Figure 9. Full-length immunoblots of co-immunoprecipitation of endogenous SF3B2, DGCR14, and RED with HA-FRA10AC1 or HA-SMU1 shown in Figure 4B

Full-length immunoblots of co-immunoprecipitation experiments performed with HEK293T cells transfected with the indicated plasmids from four independent experiments are shown. HA-SMU1 was used to co-immunoprecipitate endogenous RED (positive control). An empty vector (pMT2SM-HA) was used as a negative control. Co-precipitated endogenous splicing factors were detected by immunoblotting using anti-SF3B2, anti-DGCR14, and anti-RED antibodies. HA-tagged proteins were monitored by HRP-coupled anti-HA antibody. Red boxes indicate the cropped area.

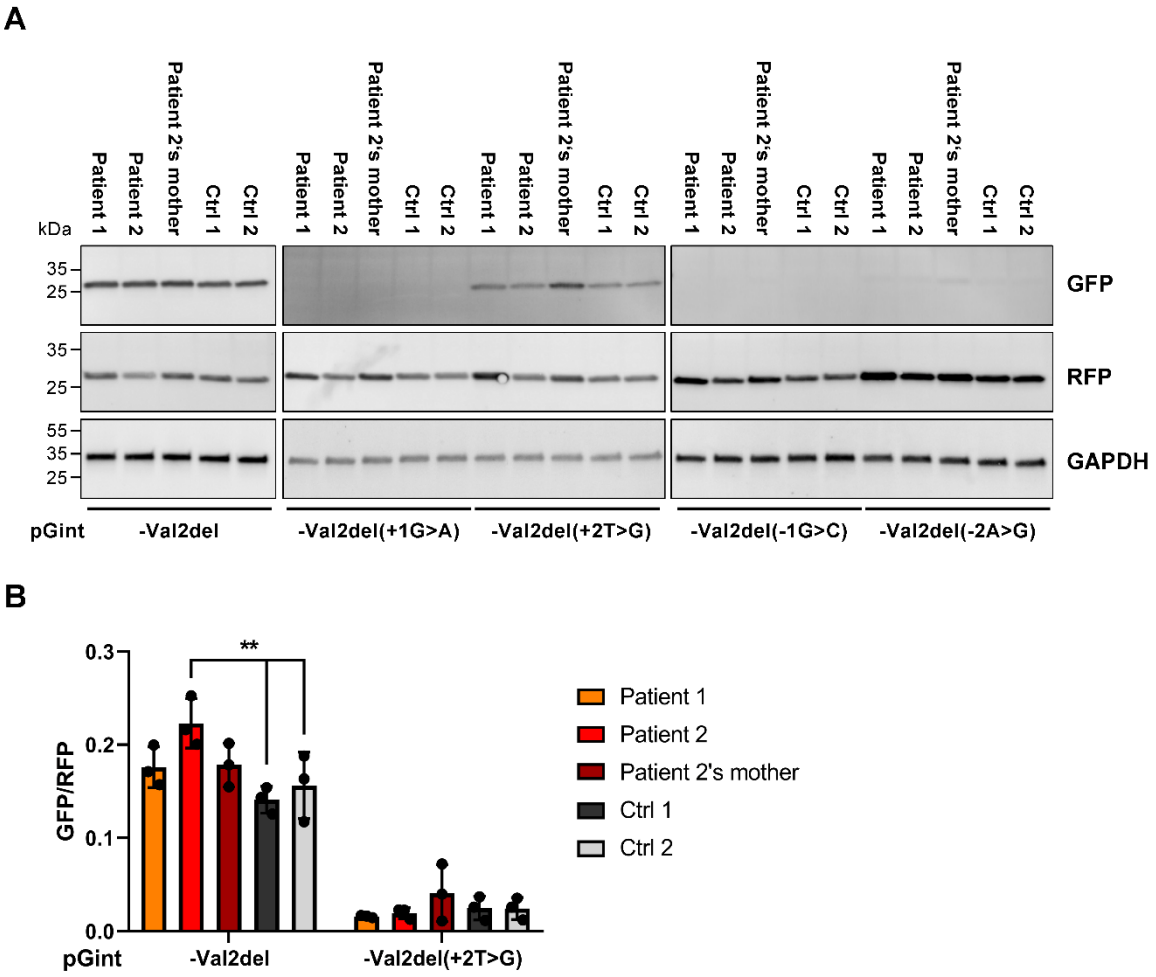

Supplementary Figure 10. Immunoblotting and quantification of EGFP after an *in vitro* splicing assay in fibroblasts

(**A**) Immunoblot of lysates from fibroblasts of patient 1, patient 2, mother of patient 2, and two controls co-transfected with the indicated pGint vector together with pmRFP-N2 plasmid. The amount of EGFP and RFP protein was monitored with an anti-GFP and anti-RFP antibody, respectively. An anti-GAPDH antibody was used to demonstrate equal loading.

(**B**) EGFP band intensities were quantified and normalized to RFP protein amount. The mean ± SD of three independent experiment is shown. Statistical significance between controls and each patient was calculated by two-way ANOVA followed by Tukey post hoc test. ** $P \leq 0.01$; Ctrl, control.

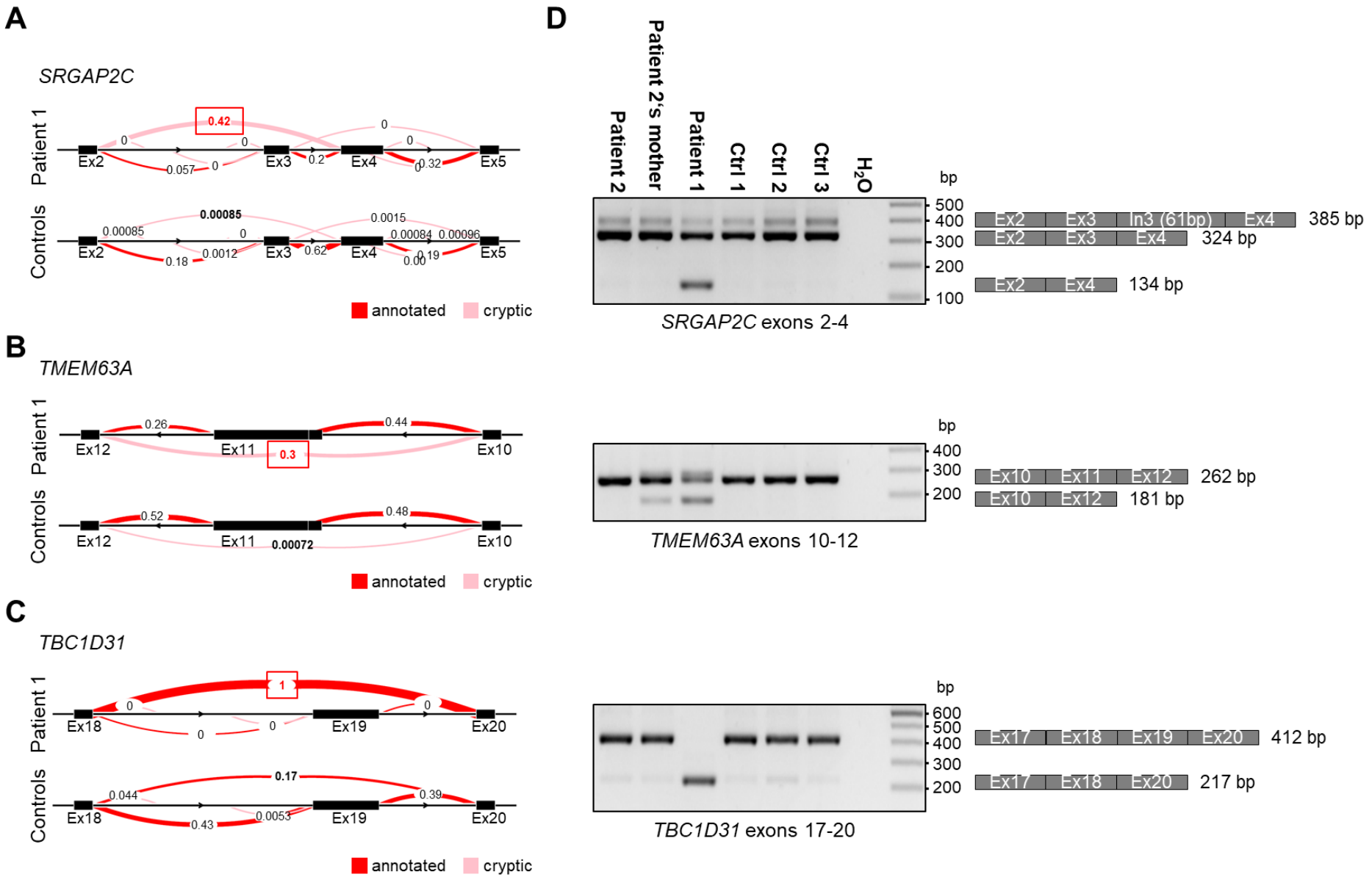
A
SRGAP2C
Patient 1
Controls
Ex2
Ex3
Ex4
Ex5
0.42
0.057
0.2
0.32
0.00085
0.0012
0.62
0.0015
0.00084
0.00096
0.19
0.00
0.18
annotated
cryptic
B
TMEM63A
Ex12
Ex11
Ex10
0.26
0.44
0.3
0.52
0.48
0.00072
annotated
cryptic
C
TBC1D31
Ex18
Ex19
Ex20
1
0.17
0.044
0.39
0.43
0.0053
annotated
cryptic
D
Patient 2
Patient 2's mother
Patient 1
Ctrl 1
Ctrl 2
Ctrl 3
H2O
bp
500
400
300
200
100
Ex2
Ex3
In3 (61bp)
Ex4
385 bp
Ex2
Ex3
Ex4
324 bp
Ex2
Ex4
134 bp
SRGAP2C exons 2-4
bp
400
300
200
Ex10
Ex11
Ex12
262 bp
Ex10
Ex12
181 bp
TMEM63A exons 10-12
bp
600
500
400
300
200
Ex17
Ex18
Ex19
Ex20
412 bp
Ex17
Ex18
Ex20
217 bp
TBC1D31 exons 17-20

Supplementary Figure 11. Alternative splicing in the *SRGAP2C*, *TMEM63*, and *TBC1D31* genes in fibroblast-derived cDNA of patient 1 and RT-PCR validation

(**A-C**) Transcriptome sequencing in fibroblast-derived cDNA identified three exon skipping events in patient 1 that were present to a lesser extent in control fibroblast-derived cDNAs. These events include skipping of exon 3 in *SRGAP2C* (**A**), skipping of exon 11 in *TMEM63* (**B**), and skipping of exon 19 in *TBC1D31* (**C**). Sashimi plots show the proportion of the detected exon-exon-junctions within patient 1's cDNA (upper panel) and controls (merged data from 41 fibroblast-derived control cDNAs, lower panel). Red lines represent annotated exon-exon-junctions and light red lines alternative (cryptic) junctions. The major alternative splicing event (proportion in patient 1) differing between patient 1 and controls is highlighted by a red frame.

(**D**) RT-PCR analysis validates all three exon skipping events in patient 1. Agarose gels are shown on the left and schematics of the exon-exon junctions as well as the expected size of the amplicons on the right. Upper panel: for *SRGAP2C* (exons 2-4), three amplicons (~380 bp, ~320 bp, ~130 bp) were present in patient 1 and two amplicons (~380 bp, ~320 bp) in patient 2, patient 2's mother, and three controls. Cloning of patient- and control-derived amplicons, *E. coli* colony PCR, and Sanger-sequencing of single colony PCR products were performed: The largest amplicon (385 bp) represents an *SRGAP2C* transcript harboring additional 61 bp of intron 3 between exons 3 and 4. The middle band (324 bp) corresponds to a transcript variant containing exons 2, 3, and 4. The smallest PCR product exclusively identified in patient 1 (134 bp) represents exon 2 directly spliced to exon 4 (skipping of exon 3). Middle panel: RT-PCR for *TMEM63A* exons 10-12. Two amplicons (~260 bp and ~180 bp) were generated from cDNA of patient 1 and patient 2's mother and one amplicon (~260 bp) from cDNA of patient 2 and three controls. Cloning of patient- and control-derived amplicons, *E. coli* colony PCR, and Sanger-sequencing of single colony PCR products were performed: The large amplicon (262 bp) corresponds to the canonical *TMEM63A* transcript variant containing exons 10, 11, and 12. The smaller band (181 bp) corresponds to a transcript lacking exon 11 (exon 10 is spliced directly to exon 12). Lower panel: A primer pair for *TBC1D31* exons 17-20 generates a single amplicon of ~220 bp in patient 1 and two amplicons of ~410 bp and ~220 bp in patient 2, patient 2's mother, and controls. Sanger-sequencing of the PCR products revealed the 412 bp-sized amplicon to correspond to the canonical transcript (exons 17-18-19-20), while the smaller band (217 bp) represents a transcript lacking exon 19 (exon 18 is spliced directly to exon 20). The three alternative splicing events in *SRGAP2C*, *TMEM63*, and *TBC1D31* were not detected in fibroblast-derived cDNA of patient 2 suggesting a *FRA10AC1*-independent effect that underlies transcript switching events in patient 1's fibroblasts. bp, base pair; Ex, exon; H_2O, water control of the RT-PCR; In, intron.

Supplementary Tables

Supplementary Table 1. Sequence of oligonucleotides and Taqman PCR Assays used in this work

Primers for amplification of *FRA10AC1* wildtype and junction fragments in family 1			
Template	**Amplicon**	**Name**	**Sequence (5' → 3')**
genomic DNA (leukocytes)	wildtype	*FRA10AC1*-In1-F	GTG AAT AGG AAT CTG CCC ACA ATG
		FRA10AC1-Ex3-R	TTC TGA AAT GGT TTT TGG AGC AG
	junction	*FRA10AC1*-5'-F	TCC TCA ACC CTG AGA AAT CTC T
		FRA10AC1-Ex3-R	TTC TGA AAT GGT TTT TGG AGC AG
***FRA10AC1* primers for variant validation in family 2**			
Template	**Intron**	**Direction**	**Sequence (5' → 3')**
genomic DNA (leukocytes)	8	forward	GCT AAT ATT CCT TTC CTT TCT GCA GG
	9	reverse	TGA GAC TTT GGG AAG CTC CA
genomic DNA (fibroblasts)	8	forward	GCA GGT CAA TTT TTC TGT GG
	9	reverse	GGG TAT ATG ATT GAT TCT TCC AAG TT
Template	**Exon**	**Direction**	**Sequence (5' → 3')**
cDNA (fibroblasts)	8	forward	CGA GTA GAA AAA GAA GTA ATT TCA GG
	11	reverse	GCA GAA GAG GCC TCC AAG A
***FRA10AC1* primers for variant validation in family 3**			
Template	**Intron**	**Direction**	**Sequence (5' → 3')**
genomic DNA (leukocytes)	7	forward	GGT GAA TGT CAT TGT TGG CTC C
	8	reverse	AAA GCA TTA TAT TCA GAC CTT TGC T
RT-PCR primers for validation of transcriptome sequencing data			
Gene	**Exon**	**Direction**	**Sequence (5' → 3')**
SRGAP2C	2	forward	GAG ATC ATA GCA GAG TAC GAT ACT
	4	reverse	GAT GTC ACT CAG GGT GGT ATG G
TMEM63A	10	forward	CTG TTC ATC ACA GGA CTC CC
	12	reverse	ACT CAC AGC CCA GCA CTT CAC
TBC1D31	17	forward	AAA TGA GAC AGC TGG AAC TCG
	20	reverse	CGG AAC TCT TTT CCT TCA GC
Predesigned Taqman PCR Assays using cDNA (Thermo Fisher Scientific)			
Gene		**Exons**	**Assay Number**
FRA10AC1		9-10	Hs00934727_m1
GAPDH		7-8	Hs02786624_g1
Primers for cloning the *FRA10AC1* coding region			
Template		**Direction**	**Sequence (5' → 3')**
cDNA		forward	CAC CAT GCA TGG TCA TGG AG
		reverse	TCA TAG AAA CAA ATC CTG AAA ATA C
Primers for cloning the *SMU1* coding region			
Template		**Direction**	**Sequence (5' → 3')**
SMU1 cDNA ORF clone (human) in pcDNA3.1+/C-(K)DYK vector		forward	TCG ACC CGG GCG GCC GCT ATG TCG ATC GAA ATC GAA TCT TCG G
		reverse	CTC CTA AAG CTC TGG AAA CCA TAA TCT AGA GAA TTC GGG G
Primers for site-directed mutagenesis of pGint			

plasmid name → plasmid name after mutagenesis	**Direction**	**Sequence (5' → 3')**
pGint → pGint-Val2del	forward	CGA GGC CAC CAT GAG CAA GGG CGA GG
	reverse	CCT CGC CCT TGC TCA TGG TGG CCT CG
pGint-Val2del → pGint-Val2del(-1G>C)	forward	CCT TTC CCT TTT TTT TCC TCA CGG CGA TGC CAC
	reverse	GTG GCA TCG CCG TGA GGA AAA AAA AGG GAA AGG
pGint-Val2del → pGint-Val2del(-2A>G)	forward	TTT CCC TTT TTT TTC CTC GGG GCG ATG CCA CCT AC
	reverse	GTA GGT GGC ATC GCC CCG AGG AAA AAA AAG GGA AA
pGint-Val2del → pGint-Val2del(+1G>A)	forward	CGG CGA GGG CGA GAT GAG TAT GGA TCC C
	reverse	GGG ATC CAT ACT CAT CTC GCC CTC GCC G
pGint-Val2del → pGint-Val2del(+2T>G)	forward	GGC GAG GGC GAG GGG AGT ATG GAT CCC
	reverse	GGG ATC CAT ACT CCC CTC GCC CTC GCC
Primers for mycoplasma detection by PCR		
Template	**Direction**	**Sequence (5' → 3')**
Cell culture supernatant	forward	GGG AGC AAA CAG GAT TAG ATA CCC T
	reverse	TGC ACC ATC CTG TCA CTC TGT TAC CCT C

Supplementary Table 2. Genetic and clinical characteristics of patients with biallelic *FRA10AC1* variants

Family/Patient	1/1	2/2	3/3-1	3/3-2	3/3-3
General information					
Gender	Female	Female	Male	Male	Male
Ethnicity	Arabic	Arabic	Arabic	Arabic	Arabic
Consanguinity	First degree cousins	First degree cousins	Second degree cousins	Second degree cousins	Second degree cousins
Genetic information					
Nucleotide change	NG_016832.1: g.4656_7575del	NM_145246.5: c.561_562insTTTA	NM_145246.5: c.494_496del	NM_145246.5: c.494_496del	NM_145246.5: c.494_496del
Amino acid change (NP_660289.2)	p.?	p.(Ser188Phefs*6)	p.(Glu165del)	p.(Glu165del)	p.(Glu165del)
Zygosity	Homozygous	Homozygous	Homozygous	Homozygous	Homozygous
Prenatal and neonatal history					
Prenatal anomalies	Heart defect; intrauterine growth retardation	Oligohydramnios; mild intrauterine growth retardation	–	–	–
Gestational age at birth in weeks + days	40+6	39	40	40	40
Birth length in cm (z-score)	48 (-1.9)	47 (-2.0)	ND	ND	ND
Birth weight in g (z-score)	3018 (-1.3)	2250 (-2.7)	2500 (-2.6)	1800 (-4.2)	2250 (-3.1)
OFC at birth in cm (z-score)	33 (-1.7)	32 (-2.5)	ND	ND	ND

Neonatal problems	Respiratory insufficiency; feeding difficulties	Feeding difficulties	–	Respiratory difficulties	–
Last examination					
Age	3 y 1 m	9 y	15 y	10 y	7 y
Height in cm (z score)	85 (-2.8)	109 (-4.3)	134 (-4.8)	113.5 (-4.2)	109 (-2.9)
Weight in kg (z score)	9.4 (-3.4)	15 (-5.3)	32 (-3.9)	20.5 (-3.6)	19 (-1.8)
OFC in cm (z score)	45 (-4.1)	47 (-4.8)	50.3 (-3.8)	49.4 (-3.1)	50 (-2.0)
Development					
Motor delay	+ (severe, nonambulatory)	+ (moderate, walking with 3 y)	–	+ (during infancy)	–
Speech delay	+ (nonverbal)	+ (nonverbal)	+ (first words with 36 m)	+ (first words with 40 m)	+ (first words with 30 m)
Intellectual disability	+ (profound)	+ (profound, IQ 35)	+ (mild, IQ 68)	+ (borderline, IQ 77)	+ (borderline, IQ 77)
Course of disease	Slow development and regression	Slow development and stationary	Slow development	Slow development	Slow development
Neurologic and psychiatric features					
Muscular hypotonia	+ (severe)	+	+	+	+
Seizures	+ (slow wave EEG)	–	–	–	–
Behavioral problems	–	+ (autistic behavior, sleep disturbance)	–	–	–

Brain abnormalities (brain ultrasound, MRI)	Corpus callosum agenesis; mild hydrocephalus internus	Partial agenesis of corpus callosum; colpocephaly; unilateral retroorbital cyst	Thin stretched corpus callosum	Thin stretched corpus callosum	Thin stretched corpus callosum
Dysmorphic features					
Face	Nevus flammeus of the forehead, nose and philtrum; broad and medial flaring of eyebrows; synophris; bitemporal narrowing; narrow palpebral fissures; hypertelorism; retrognathia; low-set dysmorphic ears; hypertrichosis	Long and triangular face; high forehead; broad and medial flaring of eyebrows; bitemporal narrowing; narrow palpebral fissures; prominent and long nose; bulbous nasal tip; long and smooth philtrum; low-set ears; lentigines	Long and triangular face; synophris; broad and medial flaring of eyebrows; narrow palpebral fissures; prominent and long nose; bulbous nasal tip; high-arched palate; thick lips; pointed chin	Long face; narrow palpebral fissures; high-arched palate; thick lips; pointed chin; dysmorphic and posteriorly rotated ears	Long face; narrow palpebral fissures; pointed chin
Malformations or anomalies					
Organ malformations	Ventricular septum defect; pulmonary atresia; hypoplastic pulmonary artery; patent ductus arteriosus; patent foramen ovale; caudally located left kidney; increased cortical signal in both kidneys; punctate echogenic foci in liver	–	–	–	–
Abnormality of the skeletal system	Short sternum; contracture of left elbow; ulnar deviation of left hand; proximal placement of thumbs; bilateral 5th finger clinodactyly	Bilateral 5th finger clinodactyly	Clinodactyly of 4th and 5th toes	Clinodactyly of 4th and 5th toes	Clinodactyly of 4th and 5th toes
Other	Feeding problems; gastric feeding tube; recurrent airway infections	Feeding problems; recurrent airway infections in early childhood	Growth hormone deficiency; anemia	Growth hormone deficiency	–

Abbreviations: +, feature present; –, feature absent; CT, computed tomography; EEG, electroencephalogram; IQ, intelligence quotient; m, months; MRI, magnetic resonance imaging; ND, no data; OFC, occipital frontal circumference; y, years.

Supplementary Table 3. ***In silico*** **pathogenicity, splice site predictions, minor allele frequency, and associated OMIM phenotypes for rare variants found in patient 1**

Chr.	Genomic position (hg 19)	Gene	mRNA reference number	Nucleotide change	Amino acid alteration	Zygosity	gnomAD browser: MAF [%]	CADD	REVEL	M-CAP	Splice site predictions	OMIM Phenotype [MIM number]	Mouse phenotype
19	48259033	*NOP53*	NM_015710.5	c.1250A>C	p.(Asp417Ala)	*de novo*	Absent	24.9	0.357	0.083	Not done	NA	Homozygous knockout is pre-implantation embryonic lethal. Heterozygous knockout reduces incidence of chemically induced skin papilloma.
2	158630612	*ACVR1*	NM_001105.5	c.631T>C	p.Leu211=	homo-zygous	Absent	NA	NA	NA	No impact	Fibro-dysplasia ossificans progres-siva [135100]	Homozygous inactivation of this gene leads to embryonic growth arrest and complete embryonic lethality due to gastrulation defects associated with abnormalities in primitive streak formation, embryonic epiblast morphology, and mesoderm and ectoderm development.
2	167760199	*XIRP2*	NM_152381.6	c.207G>C	p.(Glu69Asp)	homo-zygous	Absent	10.83	0.064	0.040	Not done	NA	Homozygous null mice exhibit severe growth retardation, abnormal myocardial fiber morphology, failure of intercalated disc maturation, cardiac conduction and ventricular septal defects, altered ionic currents in cardiomyocytes, and postnatal lethality.
3	121650557	*SLC15A2*	NM_021082.4	c.1736C>T	p.(Ala579Val)	homo-zygous	Absent	23.6	0.168	0.008	Not done	NA	Homozygous mutant mice have impairments of dipeptide transportion, however, show no gross defects.
5	176026120_ 176026143	*GPRIN1*	NM_052899.3	c.693_716del	p.(Glu233_ Lys240)del	homo-zygous	0.002335	15.3	NA	NA	Not done	NA	NA
6	160113631	*SOD2*	NM_001322816.2	c.288C>A	p.Gly96=	homo-zygous	0.002535	NA	NA	NA	No impact	{Micro-vascular	Mutations affect mitochondrial function. Null homozygotes die early with cardiomyopathy,

												compli-cations of diabetes 6} [612634]	tissue lipid accumulation, neurodegeneration, motor problems and/or metabolic acidosis depending on strain background. Heterozygotes show mitochondria and apoptosis defects with age. Inducible retina-specific conditional KO results in retinal atrophy.
10	85981888	*LRIT2*	NM_001017924.5	c.1441G>A	p.(Ala481Thr)	homo-zygous	0.007480	16.83	0.046	0.006	Not done	NA	NA
10	99079215	*FRAT1*	NM_005479.4	c.5C>G	p.(Pro2Arg)	homo-zygous	Absent	24.4	0.246	0.597	Not done	NA	NA
2	84658788	*SUCLG1*	NM_003849.4	c.674-5T>C	p.?	compound hetero-zygous	Absent	NA	NA	NA	No impact	Mitochondrial DNA depletion syndrome 9 (ence-phalomyo-pathic type with methyl-malonic aciduria) [245400]	NA
	84668238_ 84668240			c.532-12_531-10delGAT	p.?		0.002832	NA	NA	NA	No impact		

The functional impact of the identified variants was predicted by the Combined Annotation Dependent Depletion (CADD) tool, the Rare Exome Variant Ensemble Learner (REVEL) scoring system, and the Mendelian Clinically Applicable Pathogenicity (M-CAP) Score. CADD is a framework that integrates multiple annotations in one metric by contrasting variants that survived natural selection with simulated mutations. Reported CADD scores are phred-like rank scores based on the rank of that variant's score among all possible single nucleotide variants of hg19, with 10 corresponding to the top 10%, 20 at the top 1%, and 30 at the top 0.1%. The larger the score the more likely the variant has deleterious effects; the score range observed here is strongly supportive of pathogenicity, with all observed variants ranking above ~99% of all variants in a typical genome and scoring similarly to variants reported in ClinVar as pathogenic (~85% of which score >15).[12] REVEL is an ensemble method predicting the pathogenicity of missense variants with a strength for distinguishing pathogenic from rare neutral variants with a score ranging from 0-1. The higher the score the more likely the variant is pathogenic.[13] M-CAP is a classifier for rare missense variants in the human genome, which combines previous pathogenicity scores (including SIFT, Polyphen-2, and CADD), amino acid conservation features and computed scores trained on mutations linked to Mendelian diseases. The recommended pathogenicity threshold is >0.025.[14] Possible effects on splicing by intronic and synonymous variants were analyzed with the programs Human Splicing Finder 3.1, NetGene2 Server, and Berkeley Drosophila Genome Project Database.[15-18] Phenotypes of mouse models were obtained from the Mouse Genome Database (Mouse Genome Informatics, MGI).[19] Chr., chromosome; MAF, minor allele frequency; NA, not applicable.

Supplementary Table 4. ***In silico*** **pathogenicity, splice site predictions, minor allele frequency, and associated OMIM phenotypes for rare homozygous variants found in patient 2**

Chr.	Genomic position (hg19)	Gene	mRNA reference number	Nucleotide change	Amino acid alteration	Zygosity	gnomAD browser: MAF [%]	CADD	REVEL	M-CAP	Splice site predictions	OMIM Phenotype [MIM number]	Mouse phenotype
1	85331124	*LPAR3*	NM_012152.3	c.680C>G	p.(Ser227Cys)	homo-zygous	absent	28.1	0.300	0.017	Not done	NA	Homozygous null females produce smaller litter sizes and exhibit delayed implantation and altered embryo spacing that leads to delayed development of embryos and hypertrophic placentas that were shared by multiple embryos.
1	196971772	*CFHR5*	NM_030787.4	c.1308G>A	p.(Trp436*)	homo-zygous	0.003231	35	NA	NA	Not done	Nephro-pathy due to *CFHR5* deficiency [614809]	NA
1	248402952	*OR2M4*	NM_017504.2	c.722G>C	p.(Cys241Ser)	homo-zygous	0.003231	24.8	0.128	0.001	Not done	NA	NA
2	43010544	*HAAO*	NM_012205.3	c.260C>T	p.(Ala87Val)	homo-zygous	absent	25.6	0.307	0.042	Not done	Vertebral, cardiac, renal, and limb defects syndrome 1 [617660]	Mice homozygous for a knock-out allele exhibit reduced LPS-induced depressive behaviors and altered kynurenine metabolism.
2	152135361	*NMI*	NM_004688.3	c.321C>G	p.(Ile107Met)	homo-zygous	absent	25.1	0.275	0.014	Not done	NA	Conditional knockout in mammary epithelium alters mammary development and increases the aggressiveness and metastatic potential of induced mammary tumors.
2	152330547_152330549	*RIF1*	NM_001177665.2	c.7089_7091del	p.(Asn2363del)	homo-zygous	absent	19.51	NA	NA	Not done	NA	Mice homozygous for a knock-out allele exhibit embryonic lethality.
2	152484039	*NEB*	NM_004543.5	c.10141G>A	p.(Asp3381Asn)	homo-zygous	0.009686	33	0.235	0.018	Not done	Arthro-gryposis multiplex congenital 6 [619334]; Nemaline myopathy 2, autosomal recessive [256030]	Homozygous inactivation of this gene leads to stunted growth, altered sarcomere structure, reduced contractility in skeletal muscle, progressive muscle weakness, and postnatal death.

2	220379121	*ASIC4*	NM_018674.3	c.56C>T	p.(Ser19Leu)	homo-zygous	0.003236	25.3	0.221	0.039	Not done	NA	Homozygous knockout increases the fear response in the predator-odor induced fear test and increases anxiety in open field and elevated plus maze tests.
	220379630			c.565C>A	p.(Pro189Thr)	homo-zygous	absent	22.8	0.120	0.022	Not done		
3	188327580	*LPP*	NM_001167671.3	c.1061C>T	p.(Thr354Ile)	homo-zygous	absent	27.7	0.145	0.024	Not done	Leukemia, acute myeloid [601626]	Gene disruption results in fertility problems involving females but not males.
4	147741375	*TTC29*	NM_001317806.3	c.1003A>G	p.(Lys335Glu)	homo-zygous	absent	16.35	0.201	0.080	Not done	Spermato-genic failure 42 [618745]	Homozygous knockout leads to sperm flagellum malformations, resulting in reduced male fertility.
5	172113710	*NEURL1B*	NM_001308177.2	c.1450C>A	p.(Pro484Thr)	homo-zygous	absent	23.1	0.125	0.003	Not done	NA	NA
7	11675842	*THSD7A*	NM_015204.3	c.937G>C	p.(Glu313Gln)	homo-zygous	absent	22.7	0.075	0.021	Not done	NA	Targeted mutation in this gene lead to hyperactivity, impaired glucose tolerance, decreased bone mineral content, and abnormal lens and retina morphology.
7	150921072	*ABCF2*	NM_005692.5	c.496G>A	p.(Asp166Asn)	homo-zygous	0.00323	26.3	0.378	0.136	Not done	NA	NA
8	42587088	*CHRNB3*	NM_000749.5	c.638G>C	p.(Arg213Thr)	homo-zygous	absent	22.1	0.406	0.075	Not done	NA	Mice homozygous for disruptions in this gene display hyperactivity and reflex abnormalities but were otherwise phenotypically normal.
10	15600135	*ITGA8*	NM_001291494.2	c.2704C>T	p.(Leu902Phe)	homo-zygous	0.003227	19.42	0.080	0.004	Not done	Renal hypodys-plasia/ aplasia 1 [191830]	Mice homozygous for disruptions in this gene usually die by the end of the second day after birth. Those that do survive have reduced kidneys and abnormal steriocilia in the inner ear.
10	90665417	*STAMBPL1*	NM_020799.4	c.248C>T	p.(Thr83Ile)	homo-zygous	0.00323	25	0.272	0.020	No impact	NA	NA
10	93744129_ 93744131	*BTAF1*	NM_003972.3	c.2395_2397del	p.(Asn799del)	homo-zygous	absent	NA	NA	NA	Not done	NA	Embryos homozygous for an ENU-induced allele show growth retardation, edema, abnormal blood circulation, myocardial trabeculae hypoplasia, and delayed head and brain development.
10	95445066	*FRA10AC1*	NM_145246.5	c.561_562insTTTA	p.(Ser188Phefs *6)	homo-zygous	absent	32	NA	NA	Not done	NA	NA
11	46747681	*F2*	NM_000506.5	c.832G>A	p.(Gly278Arg)	homo-zygous	absent	15.00	0.343	0.091	Not done	Dyspro-thrombin-emia [613679];	Homozygotes for targeted null mutations exhibit defects in yolk sac vasculature, internal bleeding, tissue necrosis, and die in mid- to

												Hypopro-thrombin-emia [613679]; Thrombo-philia due to thrombin defect [188050]	late-gestation, or rarely, a few days after birth.
11	60183828	*MS4A14*	NM_001079692.3	c.1336G>A	p.(Glu446Lys)	homo-zygous	absent	24.8	0.232	0.013	Not done	NA	NA
11	65351226	*EHBP1L1*	NM_001099409.3	c.3083C>T	p.(Pro1028Leu)	homo-zygous	0.006478	12.41	0.070	0.032	Not done	NA	Homozygous knockout leads to a reduction in the length and density of small intestinal microvilli, severe anemia, and neonatal lethality.
12	6636176	*NCAPD2*	NM_014865.4	c.2854C>T	p.(Arg952Cys)	homo-zygous	absent	31	0.707	0.154	Not done	Micro-cephaly 21, primary, autosomal recessive [617983]	NA
13	29599566	*MTUS2*	NM_001033602.4	c.731C>T	p.(Pro244Leu)	homo-zygous	absent	15.84	0.049	0.014	Not done	NA	NA
16	67763259	*RANBP10*	NM_001320238.2	c.1276G>T	p.(Val426Phe)	homo-zygous	absent	13.66	0.086	0.016	Not done	NA	Mice homozygous for a gene trap allele exhibit slight defects in erythrocyte number and volume, decreased platelet aggregattion and increased bleeding time associated with impaired platelet dense granule release.

Rare homozygous moderate or high impact variants (e.g. missense, frameshift, splice site, and nonsense variants and in-frame duplications or deletions) with gnomAD minor allele frequencies (MAF) <0.01% and with MAFs <0.1% of the in-house database were considered. The functional impact of the identified variants was predicted by the Combined Annotation Dependent Depletion (CADD) tool, the Rare Exome Variant Ensemble Learner (REVEL) scoring system, and the Mendelian Clinically Applicable Pathogenicity (M-CAP) Score. CADD is a framework that integrates multiple annotations in one metric by contrasting variants that survived natural selection with simulated mutations. Reported CADD scores are phred-like rank scores based on the rank of that variant's score among all possible single nucleotide variants of hg19, with 10 corresponding to the top 10%, 20 at the top 1%, and 30 at the top 0.1%. The larger the score the more likely the variant has deleterious effects; the score range observed here is strongly supportive of pathogenicity, with all observed variants ranking above ~99% of all variants in a typical genome and scoring similarly to variants reported in ClinVar as pathogenic (~85% of which score >15).[12] REVEL is an ensemble method predicting the pathogenicity of missense variants with a strength for distinguishing pathogenic from rare neutral variants with a score ranging from 0-1. The higher the score the more likely the variant is pathogenic.[13] M-CAP is a classifier for rare missense variants in the human genome, which combines previous pathogenicity scores (including SIFT, Polyphen-2, and CADD), amino acid conservation features and computed scores trained on mutations linked to Mendelian diseases. The recommended pathogenicity threshold is >0.025.[14] Possible effects on splicing by intronic and synonymous variants were analyzed with the programs Human Splicing Finder 3.1, NetGene2 Server, and Berkeley Drosophila Genome Project Database.[15-18] Phenotypes of mouse models were obtained from the Mouse Genome Database (Mouse Genome Informatics, MGI).[19] Chr., chromosome; MAF, minor allele frequency; NA, not applicable.

Supplementary Table 5. Biological function and/or pathway involvement of proteins that are listed as putative FRA10AC1 interaction partners in the BioGrid database[1]

Protein function and/or involvement in a cellular pathway	Putative interactor	Original reference
Spliceosome	CHERP, CWC27, DGCR14, IK, MFAP1, NKAP, PRPF3, PRPF40A, SAP30BP, SF3B2, THOC1, TTC14, U2AF1, ZCCHC10, ZNF830	[2,3]
Metabolic pathway	ALG10B FUOM GDPD2 LPPR4	[4] [3] [5] [5]
Chloride and manganese transport, iron metabolism	ATP13A1 CLIC1 GLRX3	[4] [6] [5]
Cytoskeleton	CCDC155 MTUS2 WASF3	[7] [3] [3]
Vesicular trafficking and nuclear transport	KTN1 VPS29 XPO1	[8] [5] [9]
Cell proliferation, differentiation, MAPK signaling pathway	FGF9 MAP3K12 MOB2	[3] [5] [10]
Transcription factor	HLX	[4]
Translation elongation	EEF1D	[5]
DNA repair	ADPRHL2	[5]
Leukotriene biosynthesis	ALOX5AP	[3]
Retina morphogenesis	ROM1	[4]
Protein ubiquitination	TRIM41	[7]
Unknown protein function and/or unknown association with any pathway	C7ORF25 CCDC82 LENG1	[4] [4] [3,11]

Experimental evidence of these interactors can be found under the *Experimental Evidence Code* that supports the interaction and a publication reference (https://thebiogrid.org/125626/summary/homo-sapiens/fra10ac1.html).
Protein function and/or association with a cellular pathway were determined by use of KEGG database (https://www.genome.jp/kegg/kegg2.html), OMIM database (https://omim.org/) or uniprot database (https://www.uniprot.org/).

References

1. Oughtred R, Stark C, Breitkreutz BJ, *et al.* The BioGRID interaction database: 2019 update. *Nucleic Acids Res*. 2019;47:D529-D541.
2. Hegele A, Kamburov A, Grossmann A, *et al.* Dynamic protein-protein interaction wiring of the human spliceosome. *Mol Cell*. 2012;45:567-580.
3. Huttlin EL, Bruckner RJ, Paulo JA, *et al.* Architecture of the human interactome defines protein communities and disease networks. *Nature*. 2017;545:505-509.
4. Huttlin EL, Ting L, Bruckner RJ, *et al.* The BioPlex Network of Human Protein Interactions: Additional Unpublished AP-MS Results (Pre-Publication). *Additional Unpublished AP-MS Results from the BioPlex project, http://bioplexhmsharvardedu/* 2014.
5. Stelzl U, Worm U, Lalowski M, *et al.* A human protein-protein interaction network: a resource for annotating the proteome. *Cell*. 2005;122:957-968.
6. Wan C, Borgeson B, Phanse S, *et al.* Panorama of ancient metazoan macromolecular complexes. *Nature*. 2015;525:339-344.
7. Rolland T, Tasan M, Charloteaux B, *et al.* A proteome-scale map of the human interactome network. *Cell*. 2014;159:1212-1226.
8. Fasci D, van Ingen H, Scheltema RA, Heck AJR. Histone Interaction Landscapes Visualized by Crosslinking Mass Spectrometry in Intact Cell Nuclei. *Mol Cell Proteomics*. 2018;17:2018-2033.
9. Kirli K, Karaca S, Dehne HJ, *et al.* A deep proteomics perspective on CRM1-mediated nuclear export and nucleocytoplasmic partitioning. *Elife*. 2015;4:e11466.
10. Luck K, Kim DK, Lambourne L, *et al.* A reference map of the human binary protein interactome. *Nature*. 2020;580:402-408.
11. Huttlin EL, Ting L, Bruckner RJ*, et al.* The BioPlex Network: A Systematic Exploration of the Human Interactome. *Cell*. 2015;162:425-440.
12. Kircher M, Witten DM, Jain P, *et al.* A general framework for estimating the relative pathogenicity of human genetic variants. *Nat Genet*. 2014;46:310-315.
13. Ioannidis NM, Rothstein JH, Pejaver V, *et al.* REVEL: An Ensemble Method for Predicting the Pathogenicity of Rare Missense Variants. *Am J Hum Genet*. 2016;99:877-885.
14. Jagadeesh KA, Wenger AM, Berger MJ, *et al.* M-CAP eliminates a majority of variants of uncertain significance in clinical exomes at high sensitivity. *Nat Genet*. 2016;48:1581-1586.
15. Brunak S, Engelbrecht J, Knudsen S. Prediction of human mRNA donor and acceptor sites from the DNA sequence. *J Mol Biol*. 1991;220:49-65.
16. Desmet FO, Hamroun D, Lalande M*, et al.* Human Splicing Finder: an online bioinformatics tool to predict splicing signals. *Nucleic Acids Res*. 2009;37:e67.
17. Hebsgaard SM, Korning PG, Tolstrup N, *et al.* Splice site prediction in Arabidopsis thaliana pre-mRNA by combining local and global sequence information. *Nucleic Acids Res*. 1996;24:3439-3452.
18. Reese MG, Eeckman FH, Kulp D, Haussler D. Improved splice site detection in Genie. *J Comput Biol.* 1997;4:311-323.
19. Bult CJ, Blake JA, Smith CL, Kadin JA, Richardson JE. Mouse Genome Database (MGD) 2019. *Nucleic Acids Res*. 2019;47:D801-D806.